# Structure-Driven Nonlinear Instability as the Origin of the Explosive Reconnection Dynamics in Resistive Double Tearing Modes

M. Janvier,* Y. Kishimoto, and J. Q. Li

*Graduate School of Energy Science, Kyoto University, Uji, Kyoto 611-0011, Japan*

(Received 12 April 2011; published 31 October 2011)

The onset of abrupt magnetic reconnection events, observed in the nonlinear evolution of double tearing modes (DTM), is investigated via reduced resistive magnetohydrodynamic simulations. We have identified the critical threshold for the parameters characterizing the linear DTM stability leading to the bifurcation to the explosive dynamics. A new type of secondary instability is discovered that is excited once the magnetic islands on each rational surface reach a critical structure characterized here by the width and the angle rating their triangularization. This new instability is an island structure-driven nonlinear instability, identified as the trigger of the subsequent nonlinear dynamics which couples flow and flux perturbations. This instability only weakly depends on resistivity.

DOI: 10.1103/PhysRevLett.107.195001 PACS numbers: 52.35.Vd, 52.35.Mw, 52.35.Py, 96.60.Iv

Multiple current sheet configurations can be found in simple models of space and stellar plasmas [1,2], as well as in tokamaks with reversed magnetic shear profiles [3]. Recently, the striking phenomenon of the sudden kinetic energy onset in the double tearing mode (DTM) evolution and subsequent explosive behaviors has been found in resistive MHD simulations in cylindrical geometry [4,5]. The DTM consists of the development of plasmoids in two nearby current sheets (magnetic field discontinuity), and their associated nonlinear dynamics are of specific importance in reaching a full understanding of fast dynamics related to magnetic reconnection. Interestingly, the time scale of DTMs weakly depends on the resistivity $\eta$ once the onset takes place [6]. The phenomenon is crucial since the long-standing trigger problem leading to fast magnetic reconnection ($\sim \eta^0$ dependency) in collisional plasmas can be reproduced in a simple resistive MHD framework. Note that such a nonlinear secondary growth can also exist in $m = 1$ resistive mode [7], and accelerated reconnection evolutions were found and thoroughly investigated in [8].

Ishii *et al.* proposed a flux structure-driven nonlinear instability where the triangularization of magnetic islands and its associated current point similar to the Petschek model [4,5] play an important role. Wang *et al.*, who found similar results in slab geometry [6], showed another possibility for this universal event in terms of reconnection driven by intrinsic localized shear flows resulting from magnetic island deformation. However, the underlying physical mechanisms, particularly for the trigger leading to an accelerated growth, has not yet been unveiled.

In this Letter, we identify a new type of secondary nonlinear instability as the key role for the onset of fast reconnection. The free energy of the instability is found to be related to the two-dimensional asymmetry of the magnetic islands, so that the growth rate becomes weakly dependent on the resistivity. At the same time, we characterize a critical structure in terms of width and angle rating the deformation from which the secondary instability can be driven.

First, DTM simulations are numerically performed, based on the reduced MHD equations in slab geometry (assuming an incompressible flow and a strong magnetic guide field $B_z$ [9]), so as to obtain the evolution of $\psi$ (magnetic flux) and $\phi$ (kinetic flow). The normalization terms are the Alfvén transit time $\tau_A$ for the time variables and a characteristic unit length $a$ for the spatial ones. The equilibrium flow $\phi_0$ is 0 and the equilibrium field is the same as in [10]. Here, the two unstable current sheets exist at $x_s = \pm 0.80$ and the equilibrium current profile is kept constant to ensure a continuous linear driving force throughout the simulation. We employ a finite difference method in the $x$ direction (conducting walls at $x = \pm 5$) and a spectral method in the $y$ direction. The numerical decomposition set is $2048 \times 10$, and in the following $m = 1$ is the only linearly unstable mode. The box size in the $y$ direction is $l_y = 2\pi L_y$, and $L_y$ can be changed in order to select different wavelengths of the unstable $m = 1$ mode. The resistivity $\eta$ can be changed while the viscosity $\nu \sim 0$.

Figure 1(a) shows the nonlinear evolution of the magnetic energy ($E_M = \langle \tilde{\psi}^2 \rangle/2$, black dashed line) and kinetic energy ($E_K = \langle \tilde{\phi}^2 \rangle/2$, red plain line) of a DTM with $L_y = 0.90$. In Fig. 1(b), the instantaneous growth rate of the kinetic energy $\gamma_K = \partial_t E_K / E_K$ is also plotted. This case is typical in exhibiting explosive dynamics: after the usual exponential growth up to $t \sim 1000$ (constant $\gamma_K$), both $E_M$ and $E_K$ slow down during the Rutherford transition. This regime corresponds to the decoupling of the flow and the flux [11] such as found in tearing modes; i.e., $\phi$ almost saturates and remains quasisteady while $\psi$ grows algebraically in time as seen for $1000 < t < 4000$. Note that the instantaneous growth rate scales in this regime as $\gamma \sim \eta^1$. After this long evolution, an abrupt growth and full reconnection are found to take place during a shorter

 

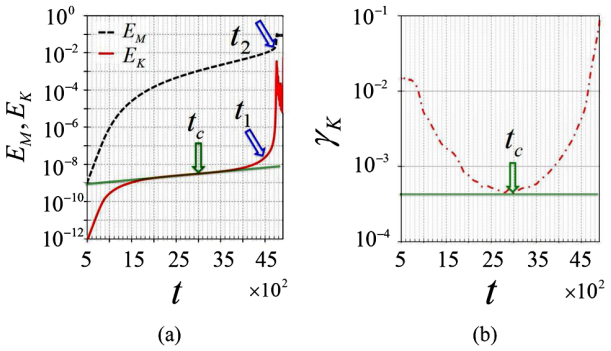


FIG. 1 (color online). (a) Time evolution for the magnetic ($E_M$) and kinetic ($E_K$) energies. At $t = t_c$, $E_K$ has an inflection point (green arrow), calculated from (b) the instantaneous nonlinear (NL) growth rate evolution $\gamma^K_{\mathrm{NL}} = \partial_t(E_K)/E_K$.

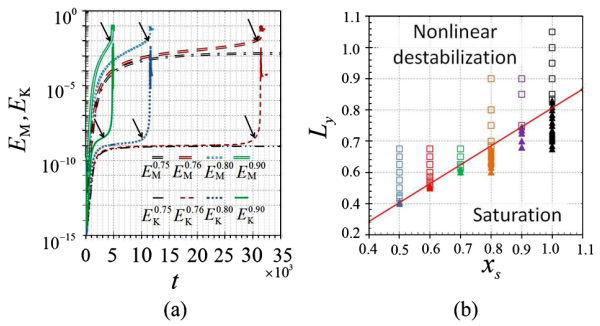


FIG. 2 (color online). (a) Time evolution of the magnetic energy $E_M^{L_y}$ (double line) and the kinetic energy $E_K^{L_y}$ (single line) for instabilities with different wavelengths $2\pi L_y$. The black arrows show the start of the explosive growth. (b) Diagram of saturated (plain triangles) and explosive DTMs (squares) obtained in function of the position of the rational surfaces ($x_s$) and the wavelength of the instability $L_y$. The solid line indicates the transition.

time scale for $4000 < t < 5000$. Checking the convergency of the simulation ensures that the latter is not numerical. This behavior confirms those found in other cylindrical and slab geometries [4,6]. Normally, the Rutherford regime is associated with decreasing $\gamma_K$ while here, at a critical time $t_c = 3000$ (green arrow), there is an inflection point in the kinetic energy evolution, calculated when $\partial_t \gamma_K = 0$ (when the second derivative of $E_K$ becomes null). This critical time may then correspond to the change in the DTM characteristics and is associated with the explosive growth clearly seen around $t_1 \sim 4500$ (blue arrow). After a delay, the growth of $E_M$ also results in an abrupt enhancement around $t_2 \sim 4700$. Assuming that there exists a causality relation $t_c < t_1 < t_2$, the increase of the kinetic flows around $t_1$ after the onset at $t_c$ must be important for triggering the second growth of the magnetic flux around $t_2$, although $E_K \ll E_M$.

To confirm this conjecture, we investigate similar dynamics for different unstable wavelengths with $L_y = 0.75 \rightarrow 0.90$, as illustrated in Fig. 2(a). As $L_y$ reduces, so does the linear growth rate, while the Rutherford regime becomes longer. The sudden growth of the energy observed in Fig. 1(a) exists as well for both $L_y = 0.8$ and 0.76 at later times but completely disappears for $L_y = 0.75$. Note that $t_c$ and $t_1$, $t_2$ defined from Fig. 1 also exist and satisfy the causality relation $t_c < t_1 < t_2$ (black arrows). More interestingly, although $L_y = 0.76$ corresponds to a 1.3% increase from $L_y = 0.75$, their evolutions are different: the explosive dynamics is triggered in the first case, whereas not in the latter for which both $E_K$ and $E_M$ saturate. This difference is clearly seen in Fig. 3 where snapshots of the magnetic flux contour are given for different times of the evolution of $L_y = 0.75$ [Fig. 3(a)] and $L_y = 0.76$ [Fig. 3(b)]. The islands stop evolving in 3(a), whereas they continue growing in 3(b) until they are structurally deformed to a triangular shape [3(b)(iii)] that allows a complete reconnection of the magnetic field lines at further times [3(b)(iv)]. These results clearly show the existence of a critical threshold in the 2D island structure leading to the bifurcation in the nonlinear dynamics.

Similar characteristics of DTMs also exist with respect to the position of the rational surfaces $x_s$ [4,12], so that we systematically explore the two-parameter space ($x_s$, $L_y$) for which the two kinds of nonlinear evolution are obtained (defined as the saturation case and the nonlinearly destabilized case). The results are plotted in Fig. 2(b), where the triangles represent saturation cases and the squares explosive DTMs. The solid line corresponds to the boundary between the two states. The nearly linear behavior of that boundary in ($x_s$, $L_y$) space suggests a similarity of the magnetic structure driving the abrupt dynamics. This gives solid grounds to the idea that the second increase of the kinetic flows around $t_c$, causing the onset of enhanced magnetic growth from $t_2$, results from the generation of a new instability, existing in a domain bounded by the solid line in Fig. 2(b). From the dynamics of the magnetic islands as discussed in Fig. 3, the development of a magnetic structure that is associated with a strong triangularization is assumed to play the role of a new free energy source for a secondary instability, marking the transition from steady configurations to explosive growths.

Now, a new methodology is proposed to confirm such an idea: we perform a linear stability analysis of equilibria with the magnetic islands obtained from the previous nonlinear simulations to disclose the secondary instability associated with the two-dimensional deformation of the islands. As the magnetic islands evolve on a long time scale during the Rutherford regime (compared to the linear or explosive growths), we can define quasiequilibria from those structures. The variables associated with such equilibria are expressed as $\psi_{\mathrm{eq}}$ and $\phi_{\mathrm{eq}}$ and the new flux and flow perturbations are written $\tilde{\psi}$ and $\tilde{\phi}$. Contrary to the standard 1D current sheet model, $\psi_{\mathrm{eq}}$ and $\phi_{\mathrm{eq}}$ are now

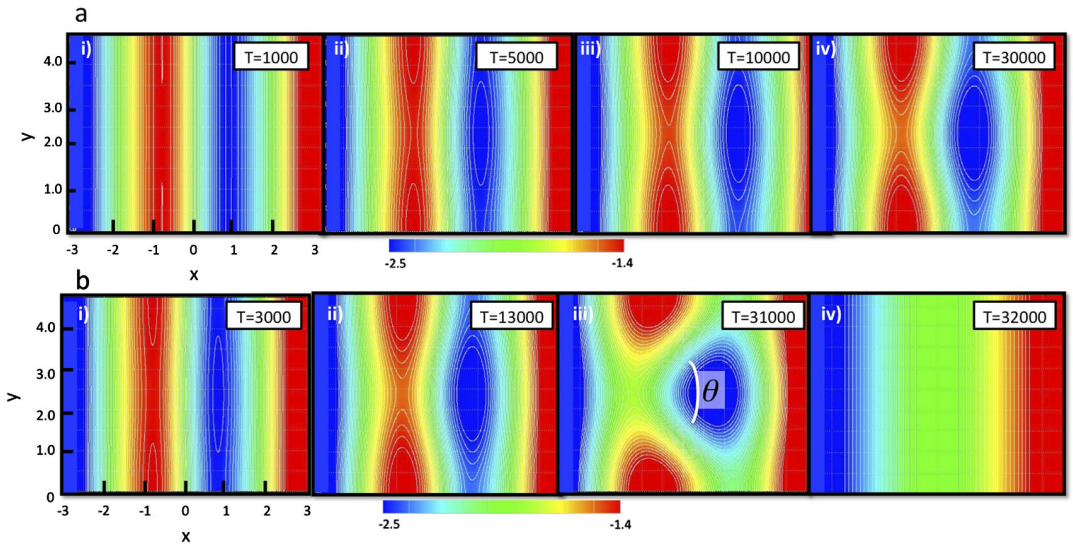


FIG. 3 (color online). Two-dimensional contour plot of the magnetic flux $\psi$ for $L_y = 0.75$ [(a), saturated DTM] and 0.76 [(b), nonlinearly destabilized DTM].

functions of both $x$ and $y$ so as to reproduce the 2D structure deformation of the magnetic field corresponding to the islands and their flows. The linearized equations are

$$\frac{\partial \nabla^2 \tilde{\phi}}{\partial t} = -[\tilde{\phi}, \nabla^2 \phi_{\mathrm{eq}}] - [\phi_{\mathrm{eq}}, \nabla^2 \tilde{\phi}] + [\psi_{\mathrm{eq}}, \nabla^2 \tilde{\psi}] + [\tilde{\psi}, \nabla^2 \psi_{\mathrm{eq}}], \quad (1)$$

$$\frac{\partial \tilde{\psi}}{\partial t} = -[\tilde{\phi}, \psi_{\mathrm{eq}}] - [\phi_{\mathrm{eq}}, \tilde{\psi}] + \eta \nabla^2 \tilde{\psi}, \quad (2)$$

where different harmonics are coupled with each other due to the Poisson brackets ($[A, B] = \partial_x A \partial_y B - \partial_y A \partial_x B$). Equations (1) and (2) determine the set of eigenfunctions ($\tilde{\psi}, \tilde{\phi}$) and the corresponding growth rate $\gamma_S$ for given equilibrium variables ($\psi_{\mathrm{eq}}, \phi_{\mathrm{eq}}$, representing DTM structures at instantaneous times of the original simulation).

To characterize the structural deformation of the quasiequilibrium magnetic islands, the couple of parameters ($w, \theta$) is chosen, corresponding to the width or angle rating the triangularization (shown in Fig. 3). Figures 4(a) and 4(b) present the evolution of $\gamma_S$ in function of $w$ and $\theta$ for $L_y = 0.75 \rightarrow 0.90$. When $(w, \theta) = (0, 180°)$, corresponding to initial sheets with no islands, the original DTM linear growth rate for each case is recovered. Looking at the evolution of $\gamma_S = f(w)$ [and also $\gamma_S = g(\theta)$], it is possible to define three phases. The first phase corresponds to the decrease of the growth rate that can be understood as follows: the current sheets are now flattened by the presence of the magnetic islands, so that the bigger those islands are, the less free energy there is to drive a current-driven instability. We refer to this region as phase I, as indicated in the graphs. For $L_y = 0.75$, where the system is subcritical for the explosive dynamics (saturated case), the growth rate $\gamma_S$ decreases from $(w, \theta) = (0, 180°)$ and becomes negative around $(w, \theta) = (0.5, 168°)$.

For cases with larger $L_y$, e.g., $L_y = 0.76$, corresponding to explosive systems, the dynamics in phase I is similar to that of $L_y = 0.75$ since the linear DTM characteristics are identical. However, beyond a stability window (indicated in Fig. 4 with red squares), $\gamma_S$ is found to increase again around $(w, \theta) = (1.1, 155°)$ as the islands grow bigger. We define this stage as phase III and the stability window as phase II. This is a strong evidence of the emergence of a new type of instability, different from that in phase I (linear DTM): since the instability appears while the free energy associated with the current sheets is minimal and cannot drive current instabilities, we can conclude that the new growth results from the development of the 2D asymmetric island deformation and we refer to it as a structure-driven nonlinearity. Note that the existence of a critical threshold for ($w, \theta$) could also be interpreted as a delicate balance

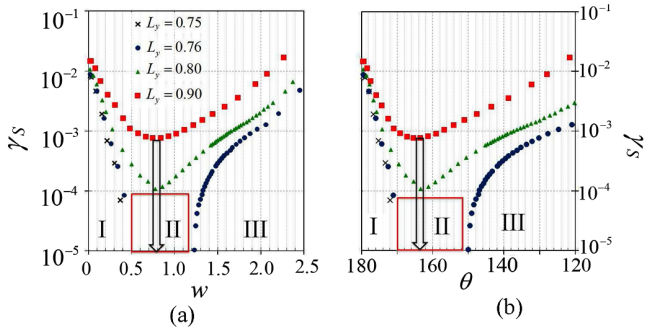


FIG. 4 (color online). Linear growth rate $\gamma_S$ of instabilities in function of (a) the equilibria island width $w$ and (b) the deformation angle $\theta$ for different wave numbers $2\pi L_y$.

between destabilizing and stabilizing forces (e.g., magnetic pressure and tension), associated with the triangularization of the islands. Further increase of $L_y$ leads to a shrunken stability window, so that for $L_y = 0.80$, it has disappeared since the resistive DTM instability (phase I) and the secondary instability (phase III) merge and overlap, showing a jump in $\partial_w \gamma_S$ and $\partial_\theta \gamma_S$ at $(w, \theta) = (0.8, 164°)$. With $L_y = 0.90$, phase I connects to phase III continuously (phase II disappears) at the inflection point of the $\gamma_S$ evolution, given as $\partial_w \gamma_S = \partial_\theta \gamma_S = 0$. The critical island parameters characterizing this threshold correspond to $w = 0.8$ and $\theta = 164°$, similar to $L_y = 0.80$.

Figure 5 presents the evolution of $\gamma_S$ in function of $w$ for $L_y = 0.9$, and $\eta$ is changed from $10^{-4}$ (red squares) to $5 \times 10^{-4}$ (blue dots). Then, the growth rate $\gamma_S$ decreases and becomes minimal around $w = 0.8$, and in this phase the slope is different depending on the resistivity. This confirms that phase I corresponds to the evolution of a current-driven instability ($\eta$ dependent). From the value $w \sim 0.8$, similar for both cases with different resistivities, the growth rate bifurcates and increases (phase III), and as the slope $\gamma_S = f(w)$ is the same for both cases, it is possible to say that phase III corresponds to the evolution of an instability weakly dependent on the diffusion term, but strongly on the structural deformation of the equilibria containing developed magnetic islands. This result is a strong confirmation that the secondary instability is not current driven. Interestingly, for well-developed and triangular islands $w > 1.2$, the relation linking $\gamma_S$ to $w$ has the form $\gamma_S \sim \exp(\beta w)$, with $\beta$ constant and independent of $\eta$.

In Fig. 6, the eigenfunction profile obtained in the phase III of the secondary instability analysis is compared with the ones from the initial DTM simulation (with $L_y = 0.90$, $\eta = 10^{-4}$). Two profiles from the $m = 1$ component of the flux and flow function, denoted $\psi_{\rm eq}$ and $\phi_{\rm eq}$, are taken at $t = 3000$ (black solid line) and $t = 4000$ (green doubled line) of the *initial* DTM. The $m = 1$ eigenfunctions $\tilde{\psi}$ and $\tilde{\phi}$ from the *secondary* analysis with a quasiequilibrium equivalent to $\psi_{\rm eq}$ and $\phi_{\rm eq}$ at $t = 3000$ are shown with the red dashed line. The amplitudes are rescaled to allow comparisons of the structural changes. From it, it is possible to say that the evolution of the DTM from $t = 3000$ to 4000 is driven by the secondary instability: the change from the eigenfunctions $\psi_{\rm eq}(3000)$, $\phi_{\rm eq}(3000)$ to $\psi_{\rm eq}(4000)$, $\phi_{\rm eq}(4000)$ indeed corresponds to the tendency given by the development of the secondary instability eigenfunctions $\tilde{\psi}$, $\tilde{\phi}$. In other words, the $m = 1$ flux and flow components $\psi_{\rm eq}$, $\phi_{\rm eq}$, found at a time $t + \Delta t$ ($\Delta t > 0$ being an arbitrary time step) of the nonlinear DTM evolution, result from the evolution of the structure at $t$ associated with the growth of the secondary instability generated by this structure at the same time. Note here that $\psi_{\rm eq}(3000)$ and $\phi_{\rm eq}(3000)$ are independent due to the decoupling between the flux and the flow in the Rutherford-like regime as discussed in Fig. 1. On the other hand, $\tilde{\psi}$ and $\tilde{\phi}$ obtained via the secondary instability analysis are coupled (linear global eigenfunction with a single growth rate $\gamma_S$). Therefore, during the evolution from $t_c \sim 3000$ to $t_1 \sim 4000$ (Fig. 1), the independent variables ($\psi_{\rm eq}$, $\phi_{\rm eq}$) become dependent, resulting in global characteristics at $t = 4000$. This subsequent coupling between the flux and the flow is considered to play an important role in enhancing the spontaneous growth rate observed from $t_1$ to $t_2$.

So far, we have shown that the spontaneous secondary growth in the nonlinear development of DTMs is linked to the generation of a secondary instability, developing to exhaust the free energy associated with the magnetic island structure. Now, on one hand, the evolution of the island width is found to be $w \sim t$ in the Rutherford-like regime of DTMs. On the other hand, from phase III in Fig. 4(a), the growth of the secondary instability for a given equilibrium is written $\gamma_S \sim \exp(\beta w)$. The relation $\gamma_S \sim \exp(\beta t)$ is then deduced linking $\gamma_S$ to the instantaneous time evolution of the original DTM. From the critical time $t_c$, potential flows are then expected to evolve instantaneously as

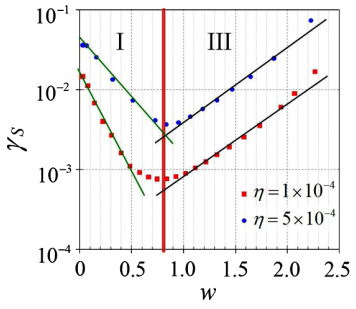


FIG. 5 (color online). Linear growth rate $\gamma_S$ of the perturbation for $L_y = 0.90$ in function of the quasiequilibria islands width $w$, for $\eta = 10^{-4}$ (red squares) and $5 \times 10^{-4}$ (blue circles).

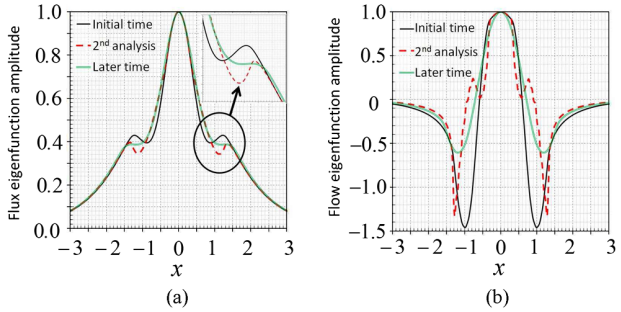


FIG. 6 (color online). Profiles of (a) $\psi$ (flux) and (b) $\phi$ (flow) eigenfunctions of the original DTM at $t = 3000$ (black solid line) and $t = 4000$ (green doubled line) compared with the secondary instability analysis eigenfunction (red dashed line) corresponding to $t = 3000$ of the original DTM.

$\phi \sim \exp(\gamma_S t) \sim \exp(e^{\alpha t} t)$, exhibiting an explosive fast growth as formerly seen in Fig. 1(a). Once secondary flows are triggered, successive nonlinear coupling chains establishing a positive feedback loop are expected: $\tilde{\phi}$ and $\psi_{\mathrm{eq}}$ (where $\psi_{\mathrm{eq}}$ denotes the 2D magnetic structure at time $t$) couple through the Poisson brackets $[\tilde{\phi}, \psi_{\mathrm{eq}}]$, enhancing $\tilde{\psi}$ which subsequently triggers the magnetic flux at $t = t_2$ [Fig. 1(a)]. Then, the enhanced $\tilde{\psi}$ further accelerates $\tilde{\phi}$ through the Maxwell stress $[\tilde{\psi}, \nabla^2 \tilde{\psi}]$, leading to the abrupt full reconnection as shown in Fig. 3 for $L_y = 0.76$. Note that this process exists along with the coupling between the flux and the flow leading to a globalization of the mode structure as discussed in Fig. 6. During the fast explosive growth, the magnetic and kinetic energies of the global mode are still sustained by the time independent 1D current equilibrium gradient at the rational surfaces.

In this Letter, we investigated the origin of the trigger of the sudden explosive magnetic reconnection in the DTM in a slab geometry with a strong guide field. By means of a secondary instability analysis of the quasisaturated equilibria obtained during the nonlinear DTM, we found for the first time that the onset consists in the development of a new type of instability whose free energy is ascribed to the slowly evolving 2D magnetic island deformation. The following growth of the potential flow due to this secondary instability is found to be essential in leading the explosive reconnection dynamics though its energy level is low compared with that of the magnetic flux. We also found that the secondary instability shows a weak resistivity dependency compared with that of the linear DTM. Considering that the instability is induced intrinsically from the slow time scale evolution of the system, this structure-driven nonlinear instability is expected to play a key role in understanding the physical mechanism of the onset of sudden and fast magnetic reconnection events, a long-standing problem in solar or space physics and magnetically confined fusion plasmas.

This work was supported by a Grant-in-Aid from JSPS (No. 21340171).

*Corresponding author.
janviermiho@gmail.com

[1] M. Yan *et al.*, J. Geophys. Res. **99**, 8657 (1994).
[2] R. B. Dahlburg and J. T. Karpen, J. Geophys. Res. **100**, 23489 (1995).
[3] C. Gormezano, Plasma Phys. Controlled Fusion **40**, A171 (1998).
[4] Y. Ishii, M. Azumi, and Y. Kishimoto, Phys. Rev. Lett. **89**, 205002 (2002).
[5] Y. Ishii *et al.*, Phys. Plasmas **7**, 4477 (2000).
[6] Z. X. Wang *et al.*, Phys. Rev. Lett. **99**, 185004 (2007).
[7] A. Y. Aydemir, Phys. Rev. Lett. **78**, 4406 (1997).
[8] M.-C. Firpo and B. Coppi, Phys. Rev. Lett. **90**, 095003 (2003).
[9] H. R. Strauss, Phys. Fluids **19**, 134 (1976).
[10] P. L. Pritchett *et al.*, Phys. Fluids **23**, 1368 (1980).
[11] P. H. Rutherford, Phys. Fluids **16**, 1903 (1973).
[12] A. Bierwage *et al.*, Phys. Plasmas **14**, 022107 (2007).